Bioactive Materials 10 (2022) 236–246

Contents lists available at ScienceDirect

Bioactive Materials

journal homepage: www.keaipublishing.com/en/journals/bioactive-materials

3D-printed dermis-specific extracellular matrix mitigates scar contraction via inducing early angiogenesis and macrophage M2 polarization

Lei Chen [a], Zhiyong Li [b], Yongtai Zheng [b], Fei Zhou [a], Jingling Zhao [a], Qiyi Zhai [a], Zhaoqiang Zhang [c], Tianrun Liu [d], Yongming Chen [b,**], Shaohai Qi [a,*]

[a] Department of Burns, Laboratory of General Surgery, The First Affiliated Hospital, SunYat-Sen University, Guangzhou, 510080, China
[b] School of Materials Science and Engineering, Centre of Functional Biomaterials, Key Laboratory of Polymeric Composite Materials and Functional Materials of Ministry of Education, GD Research Centre for Functional Biomaterials Engineering and Technology, Sun Yat-sen University, Guangzhou, 510275, China
[c] Department of Oral and Maxillofacial Surgery, Stomatological Hospital, Southern Medical University, No. 366, South of Jiangnan Boulevard, Guangzhou, 510280, China
[d] Department of Otorhinolaryngology Head and Neck Surgery, The Sixth Affiliated Hospital of Sun Yat-sen University, Guangzhou, Guangdong, China

ARTICLE INFO

Keywords:
Extracellular matrix
Dermal analogues
Scar contraction
Macrophage
Angiogenesis

ABSTRACT

Scar contraction frequently happens in patients with deep burn injuries. Hitherto, porcine dermal extracellular matrix (dECM) has supplied microenvironments that assist in wound healing but fail to inhibit scar contraction. To overcome this drawback, we integrate dECM into three-dimensional (3D)-printed dermal analogues (PDA) to prevent scar contraction. We have developed thermally gelled, non-rheologically modified dECM powder (dECMp) inks and successfully transformed them into PDA that was endowed with a micron-scale spatial structure. The optimal crosslinked PDA exhibited desired structure, good mechanical properties as well as excellent biocompatibility. Moreover, *in vivo* experiments demonstrated that PDA could significantly reduced scar contraction and improved cosmetic upshots of split thickness skin grafts (STSG) than the commercially available dermal templates and STSG along. The PDA has also induced an early, intense neovascularization, and evoked a type-2-like immune response. PDA's superior beneficial effects may attribute to their desired porous structure, the well-balanced physicochemical properties, and the preserved dermis-specific ECM cues, which collectively modulated the expression of genes such as *Wnt11, ATF3,* and *IL1β,* and influenced the crucial endogenous signalling pathways. The findings of this study suggest that PDA is a clinical translatable material that possess high potential in reducing scar contraction.

1. Introduction

Burns are the fourth most common cause of trauma following traffic accidents, falls, and intentional injuries. Statistics show that there are more than a million burn patients in the United States each year, and the relevant treatment costs are up to 4 billion U.S. dollars [1]. Apart from shock and sepsis, scar contraction is also one of the most serious complications of burns, with the incidence ranging from 30% to 90% [2,3]. The firm red scars continue to grow and contract within 1 or 2 years after injury, causing damage to the patient's appearance and severely affecting their physical activities, and finally resulting in emotional trauma and skill loss. Therefore, preventive treatment is one of the current research hotspots of clinical study and regenerative medicine research.

State-of- the-art burn care to prevent scar contraction involves early grafting or flap transfer [4]. However, these preventive therapies could cause cicatricial contracture at the donor or flap site, and are often affected by insufficient skin/flap sources or knock-on psychosocial impact. Recently, injectable hydrogels and 3D bio-printing techniques has been focused on producing skin substitutes to replace cells lost at the defect site. Studies have shown that mesenchymal stem cells loaded dermal patches, double-layer bionic skin and pre-vascularized 3D printed skin can significantly accelerate wound closure [5,6]. However, most studies focused on material mediated cellular responses *in vitro*, rather than macroscopic process of wound healing [7]. There is

Peer review under responsibility of KeAi Communications Co., Ltd.
* Corresponding author.
** Corresponding author.
E-mail addresses: chenym35@mail.sysu.edu.cn (Y. Chen), qishh@mail.sysu.edu.cn (S. Qi).

https://doi.org/10.1016/j.bioactmat.2021.09.008
Received 28 May 2021; Received in revised form 21 August 2021; Accepted 4 September 2021
Available online 22 September 2021

Abbreviations

3D	three-dimensional
CCR7	C–C-motif chemokine receptor 7
CD163	cluster of differentiation 163
CD68	cluster of differentiation 68
dECM	dermal extracellular matrix
dECMp:	dECM powder
FTSGs	full-thickness skin grafts
ECM	extracellular matrix
GA	glutaraldehyde
GO	gene ontology
HUVEC	human umbilical vein endothelial cell
IS	inguinal split-thickness skin grafts
KEGG	Kyoto Encyclopaedia of Genes and Genomes
LPS	lipopolysaccharide
MTT	3-(4,5- dimethylthiazol-2-yl)-2,5-diphenyltetrazolium bromide
Mϕs	macrophages
PDA	3D-printed dermal analogues
PL:	Pelnac Dermal Substitute
qRT-PCR	quantitative real-time polymerase chain reaction
RNA-seq	RNA-sequencing
SEM	scanning electron microscopy
STSGs	split-thickness skin grafts

insufficient evidence and controversies at present to support the role of the biomaterials in inhibiting scar contracture. For example. Immunodeficiency animal models are often used for *in vivo* verification, which ignores the importance of immune response to both scar contraction and material success. The implanted materials are easy to become dry and inactivated due to the evaporation, so the wounds are mainly closed by centripetal contracture [8,9]. In addition, the skin substitutes also have issues related to the cell therapy, including the selection of cell category and materials, the maintenance of cell viability before and after the printing, and *in vitro* air-liquid interface/bioreactor culture. As a result, the clinical application of these materials is hindered by the factors such as long preparation time, high cost, short shelf time (only 15 days), and the difficulties in overall quality control.

Regeneration guiding scaffolds could stimulate pro-healing or immunomodulating behaviors of *in situ* cells, which avoided complex processing through using the activity of the material itself than that of the cells. Natural polymer materials such as Pelnac® and Integra® are this certain type of products [10,11]. During surgery, autologous split skin graft will be placed on top of the tissue engineered dermal substitute to enable wound repair and inhibit scarring. The possibility of the scar conctration of the wounds repaired by this classic surgical method is closely related to whether the material triggers excessive inflammation and whether the dermal matrix can obtain adequate blood supply from the underlying wounds [12–14]. Porcine dermal extracellular matrix (dECM) is biocompatible and also similar to human skin in terms of composition and immunology, thereby has been used for years to repair wounds [15]. Generated through the continuous dynamic interactions between its resident cells [16], dECM retains the intrinsic cues of the native tissue including paracrine signalling molecules. Research confirms that dECM could be formulated into injectable hydrogel, which can *in-situ* promote wound healing through its own biological activity [17]. However, prior studies reported that the extraction of dECM from natural skin usually requires longer physical, chemical and enzyme processes, which not only destroys the mechanical properties of the material, but also entailed a concurring risk of degrading the matrix [18]. Therefore, the complexity of preparation and the instability of materials should not be ignored.

To solve the issues brought up by above bottom-up approaches, the soluable powder (dECMp) was prepared by mechanically disrupting dECM, which completely maintained the composition of dECM and submicron surface morphology, resulting in the good interaction between the materials and wound-repairing cells. In this study, we developed thermally gelled, non-rheologically modified dECMp inks to construct a novel 3D-printed cell free dermal analogue (PDA), which has microporous structure with 100% connectivity. The combined transplantation of PDA and autologous STSG significantly promoted the repair of full-thickness skin wounds and inhibited scar contraction, due to its immune regulation and early vascularization properties. As far as we know, this study is the first report that maximumly transforms the porcine cell-free materials into the skin substitutes through a simple and effective 3D printing technology.

2. Materials and Methods

The detailed and expanded Materials and Methods section is available in the Supporting Information.

3. Results and discussion

3.1. Preparation and characterization of dECMp

ECM provides both tissue-specific ultrastructural support and functional molecules that influence local cell behaviour. Compaired with enzyme-based extraction, mechanical disruption of the dECM could avoid material degradation and lower the processing costs. As shown in the first column of Fig. 1A, native porcine dermis samples were crushed into ultrafine, dry dECMps. By DAPI staining, the absence of cells or of necrotic cell debris were confirmed in the dECMps (the second column of Fig. 1A). The residual DNA amounted only to $2.34 \pm 0.18\%$ mg^{-1} dECMp dry weight in Fig. 1B. Thus, there would be little inflammatory reaction at this depleted concentration.

As the results gained via Masson's Trichrome (the third column of Fig. 1A) and toluidine blue staining (the fourth column of Fig. 1A), both collagen and GAGs were well preserved in the dECMps. More than 200 unique protein species could be identified by mass spectrometry analysis in our dECMps (see Table S2, and Figs. S1 and S2). The preserved proteins could provide critical matrix cues that would promote cell attachment and advance tissue regeneration [19–21]. Because of the removal of the cellular components and water, the collagen content increased proportionately ($312.07 \pm 9.01\%$; $p < 0.05$), compared to the native tissue in Fig. 1C. Conversely, the GAGs content moderately decreased ($61.15 \pm 6.49\%$; $p < 0.05$), compared to the native tissue in Fig. 1D.

3.2. Characterization of dECMp ink and PDA

The rheological test were performed to devise the optimized formula of the ink with different dECMp weight concentrations (wt. %) of 8.0, 8.5, and 9.0, respectively. Both the elastic modulus (G′) and the loss modulus (G″) were strongly temperature dependent in Fig. 2A, because (1) the optimum temperature of the ink container during the printing was 18–20 °C, which allowed for smooth, continuous, controllable, and uniform extrusion through the nozzles; and (2) the optimum temperature of the printing platform after deposition was 4 °C, which favoured fast gelation and structure maintenance. Notably, since the ink with a dECMp concentration of 8.5 wt% had the highest G'and G″ moduli values, it was chosen for fast temperature-controlled, layer-by-layer 3D-printing.

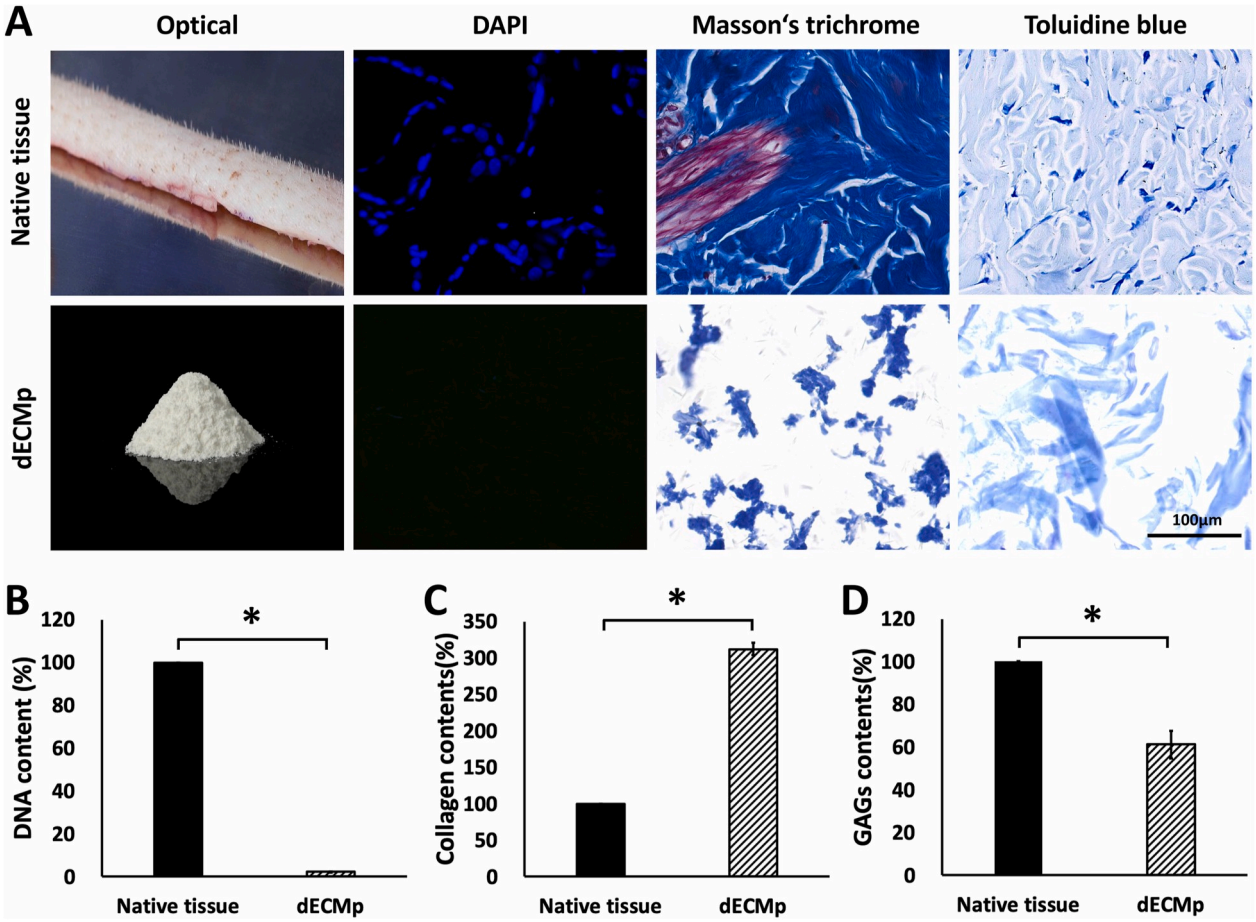

Fig. 1. The decellularization and the biochemical analysis of the native porcine skin samples. (A) The optical and the microscopy pictures of the native porcine skin and the dECMp stained with DAPI, Masson's trichrome, and toluidine blue. The contents of (B) DNA, (C) Collagen, (D) GAGs in the native tissues and the dECMp. *$p < 0.05$.

Glutaraldehyde (GA) solutions with different concentrations were used to crosslink the ink as shown in Fig. 2B. By adjusting the GA concentration among 0.1 and 1.0 wt%, the G′ modulus ranged from 10 kPa to 100 kPa, while when the concentration was 0.1 wt%, the low G′ and G″ moduli of the ink hindered the dECM printing. The maximum G′ and G" values were reached at 0.25 wt%, but when the GA density increased further, G′ and G″ decreased. Meanwhile, the thermal sensitivity change of the crosslinked ink could be due to the crosslinking between molecular chains [22,23], which was a prerequisite for maintaining the 3D-printed constructs further on.

The mechanical properties of the stent are critical to its operability in clinical use. The tensile test results showed that under the tensile loading, the nominal stress/strain values increased up to the breaking point, except for the 0.25 wt% crosslinked ink (Fig. 2C). On the one hand, the increased GA concentration strengthened the tensile strength of the material. On the other hand, the strong tensile strength made the stent brittle. Further, considering the high concentration of GA will affect the biocompatibility of the printed dermis, we chose 0.25 wt% GA to cross-link the scaffold.

Therefore, the ink with a dECMp concentration of 8.5 wt%, and a GA concentration of 0.25 wt% were applied to quickly print shape-controlled constructs (PDAs). Fig. 2D showed dECMp inks (before crosslinking) at gel (4 °C) and pre-gel (20 °C) phases. Fig. 2E showed the porous network structure of PDA (outer dimension, 20 mm × 20 mm). Degradation experiments proved that the PDA could maintain a stable for up to 56 days (Fig. 2F). The biocompatibility of the printed scaffolds was investigated by seeding L929 fibroblasts on the surface of PDAs. SEM scanning showed the designed porous 3D structure of PDA (mean pore diameter is 131.2 ± 96.8 μm, similar to that of the human acellular dermal matrix) with attached, well spreading L929 fibroblasts (Fig. 2G). We further employed the Live/Dead cell staining for further visualization of the cell viability [24]. As shown in Fig. 2G, L929 fibroblasts (green fluorescently dyed) were proliferated healthily on the PDAs. MTT assay were applied to quantified the viability of L929 fibroblasts incubated in PDA-conditioned media using the fresh culture medium as the control. The results (Fig. 2H) revealed that the viability of L929 fibroblasts cultured in media containing either 75% (134.19 ± 5.34) or 100% (141.60 ± 6.93) PDA extracts was higher than that of the fresh medium-exposed control group ($p < 0.05$). Altogether, crosslinked PDAs displayed a good cytocompatibility *in vitro*.

3.3. Skin grafts contraction

A clinically relevant, immune competent rat STSG model [25] was used to assess the therapeutic efficacy of PDA *in vivo*. Pelnac® (single layer, Gunze, Japan), a swine-origin standard implantable artificial dermis was applied as the positive control. The schematic diagram of the surgical procedure was shown in Fig. 3A. Considering the time that the scar contraction of grafted wounds required to develop, the morphological changes and the contraction of the wounds (Fig. 3B and C) in the rats treated with inguinal STSG (IS, obtained as previously reported [26]), Pelnac® + IS (PL), or PDA + IS (PDA) were followed for up to 28 days after the operation [27]. At the post-operative 7th day, while the grafts in the PDA group were flat, coloured, and firmly attached to the recipient's bed, the grafts of the remaining groups already exhibited erosions, exudates, local signs of ischemia, and undesquamated crusts

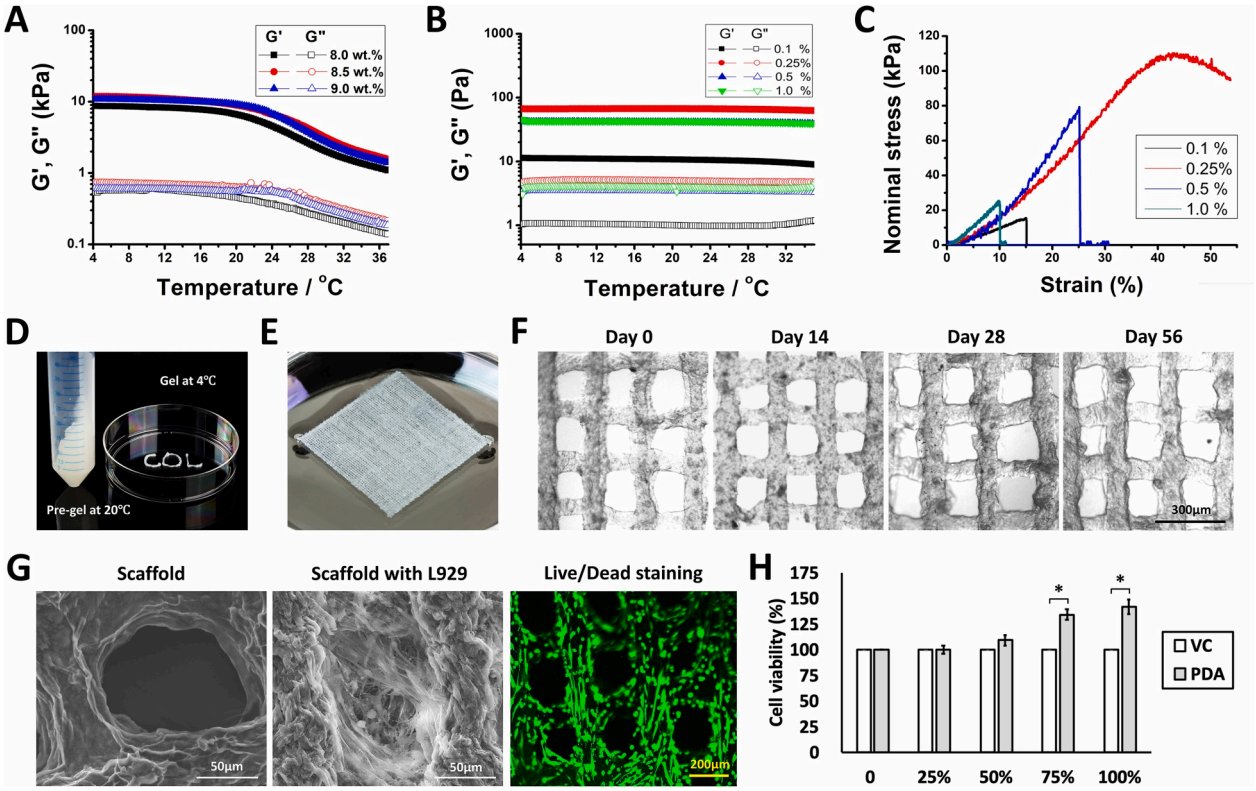

Fig. 2. (A) The temperature dependence of the elastic modulus (G′) and the loss modulus (G″) of the print inks with different collagen concentrations. (B) The G′ and G″ temperature dependence the dECMp ink (at the concentration of 8.5 wt%) crosslinked with GA of 0.1, 0.25, 0.5, and 1.0 wt%. (C) The nominal stress and strain relationship of the crosslinked dECM inks. (D) The gel-to-pre-gel transition of the dECMp ink. (E) A PDA sample. (F) Evaluation on the PDAs' morphological structure for 56 days of incubation *in vitro*. (G) Representative SEM images of PDAs with or without L929 fibroblasts, and representative Live/Dead images of L929 fibroblasts cultured on PDA. *Green*: live cells. *Red*: dead cells. (H) MTT assay of L929 fibroblasts viability. The percentage of viable cells were calculated as ODs ratios between the PDAs extracts-treated cells and the control cells, $^{*}p < 0.05$.

which indicated unstable and immature graft takes. However, since the post-operative 14th day onwards, the PDA group significantly inhibited in comparison with the other groups grafts contraction (97.61 ± 6.31%, $p < 0.05$). The redness of the PDA grafts progressively faded with time and the dissimilarities between the PDA grafts and the surrounding skin diminished. The greatest contraction differences occurred at the 28th day between the PDA (87.21 ± 4.17%) and PL (57.22 ± 1.73%) groups ($p < 0.05$ in both instances), while the grafts of the IS groups presented a modest degree of shrinkage. Overall, the PAD were neatly superior to IS and PL grafts in lessening scar contraction and in improving cosmetic wound healing upshots. Compared with the majority of tissue enigeered products focusing on stimulating repaid wound healing, PDA we designed would be more suitable to combat scar contraction in patients large-area skin defect.

3.4. Corresponding transcriptome analyses

The above results showed that there were significant differences between the PDA and PL groups. The superior therapeutic effectiveness of PDAs could be due not only to the paracrine signalling molecules stored in the dECMp, but also to a deft and proper balance between chemical modifications and biophysical qualities [28]. Hitherto, only a small number of studies [29,30] have systematiclly analyzed the gene expression profiles of skin substitutes. Given the complexity of these two materials, transcriptome analyses were performed to reveal the transcription to underpin the above conspicuous changes. The heat maps of the differently expressed genes were shown in Fig. 4A. In comparison with the PL group, on the 7th day, 179 genes were significantly up-regulated and 457 genes down-regulated in the PDA group; while on the 28th day, in the PDA group 110 genes were significantly up-regulated and 528 genes down-regulated.

We applied Gene ontology (GO) and pathway enrichment analyses to track down the biological processes and metabolic and/or signalling pathways involved by the above differently expressed genes. Thus, the differential genes of PL-*vs.*-PDA groups on the 7th day were significantly enriched regarding 86 GO terms and 59 signalling pathways. On the 28th day, the differential genes of PL-*vs.*-PDA groups were significantly enriched with respect to 122 GO terms and 31 signalling pathways. At the selected time points, the differently expressed genes of the two groups under comparison were mainly enriched with reference to biological entities or processes such as Z disc, M band, myofibril, muscle contraction, and so on.

Further, the Kyoto Encyclopaedia of Genes and Genomes (KEGG) analysis showed that the differently expressed genes were mainly enriched as regards oxytocin signalling pathway, cardiac muscle contraction, gastric acid secretion, and so on. Fig. 4B and C illustrated the top enriched GO terms and KEGG pathways pertaining to each group respectively. Among them: insulin secretion was previously reported not only as a potent chemoattractant and mitogen for cells involved in wound healing, but also as being capable of promoting keratinocyte growth and of collagen synthesis by fibroblasts [31]; the oxytocin signalling pathway was proven to regulate endothelial cell proliferation, stimulate angiogenesis [32,33], and mediate new blood vessel formation [34,35]; the Jak-STAT signalling pathway was considered as one of the most important signalling pathways in regulating inflammation reaction and fibrosis [36,37]; the chemokine signalling pathways was found to induce neovascularization and relate to the progression of hepatic fibrosis [38,39]; tight junction [40], focal adhesion [41,42] and MAPK signalling pathway [43,44] were reported as the pathways that highly associated with collagen deposition and fibrosis [42,45–47]. The above

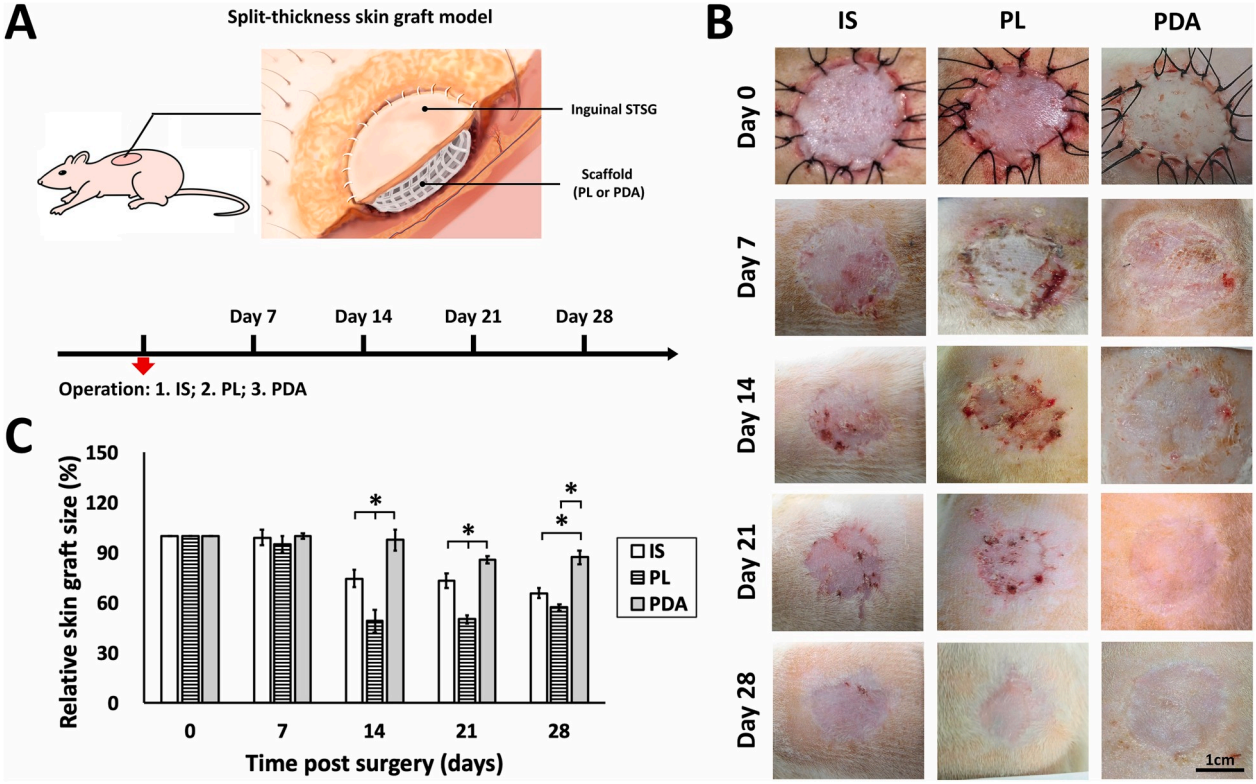

Fig. 3. (A) Full thickness skin defects were classed into three groups: IS, PL, and PDA. Evaluations were performed at the selected post-operation days. (B) The morphological changes occurring in the diverse types of skin grafts (i.e. IS, PL, and PDA) during the first 28 days after the surgery. (C) The quantification of relative skin graft size, $*p < 0.05$.

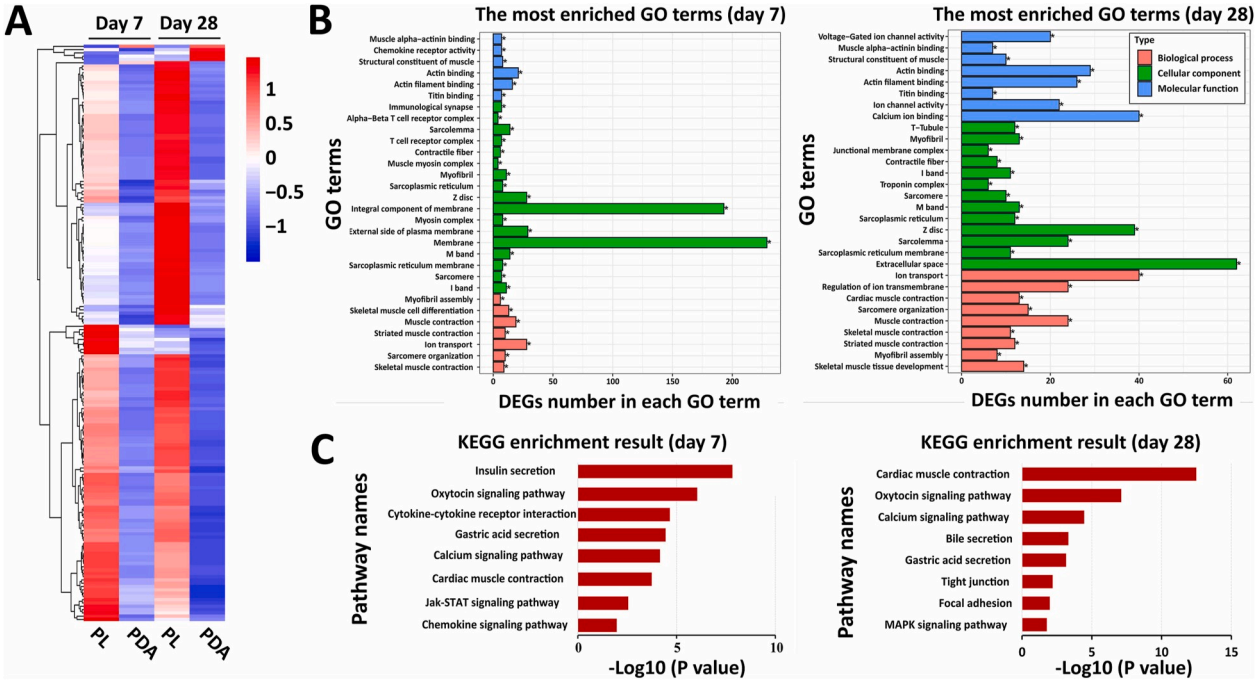

Fig. 4. (A) The heat map of the differential expression of several genes. The ordinate indicates the relative expression levels of the genes that are intersected (z-score scaling on mean value of FPKM). *Red* indicates a higher gene expression level, whereas *blue* specifies a lower gene expression level. High ⇒ low gene expression is represented by a change of colour from *red* to *blue*, respectively. (B) GO enrichment analysis of the differentially expressed genes. The top 30 enriched terms: the abscissa indicates the number of genes enriched on the GO Term; the bars are variously coloured to distinguish biological processes, cellular components, and molecular functions; marks a significantly enriched GO Term; from left to right, panels represent the compared groups on the 7th day and the 28th day post-operatively. (C) KEGG pathway enrichment analysis: the ordinate shows the name of the significantly enriched pathway, while the abscissa specifies the $-\text{Log}_{10}$ (p-value); from left to right, panels represent the compared groups at the 7th day and the 28th day, *corrected $p < 0.05$.

results indicated that the difference in the phenotype of animal wounds between the PL and PDA groups was caused by a series of changes in the wound cells at the genetic level mediated by the material (Fig. S3 shows qRT-PCR expression pattern validation of transcriptome data in the PL and in PDA groups).

It was worth noting that some conventional wound repair-related signalling pathways, such as the Wnt, PI3K-Akt, and TGF-ones, were not differentially enriched in PL-*vs.*-PDA groups, which might be due to shared treatments like wounding and skin grafting in these two groups did not induce the significant difference in transcription of related genes.

3.5. The skin graft changes after the surgery and the collagen deposition and maturation

The differentiation of an abnormal keratinocytes activates the fibroblasts, thus partaking in the promotion of the tissue fibrosis and contraction [48,49]. The H&E staining allows us to analyse structural changes within the graft epidermis. As shown in Fig. 5A and B, on the 7th day, the epidermis almost regained its original appearance in IS and PDA groups, while epidermal hyperplasia and exfoliation were manifest in PL group. On the 14th day, a distinctly thickened epidermis was apparent in PL (130.51 ± 7.49 μm) and IS (50.10 ± 4.04 μm) grafts. Over time, due to wound remodelling, the thickness of the newly formed epidermis significantly decreased in all groups. On the postoperative 28th day, the epidermis over PDA grafts was almost fully restored to a normal morphology (25.85 ± 3.89%), while the grafts of PL group still showed an epidermal hyperplasia (66.38 ± 4.28%, $p < 0.05$).

Hair follicles and their annexed sebaceous glands amounted to relevant components of a reconstituted skin. Fig. 5C and D showed the corresponding results. On the 7th day the PDA grafts had mostly conserved a uniform distribution of hair follicles (30.67 ± 3.06), while a few of them (5.00 ± 2.00, $p < 0.05$) had remained in the PL grafts. From the 14th day to the 28th day, as the remodelling progressed, the hair follicles numbers kept falling. The grafts belonging to the PDA group still exhibited a close resemblance to the normal epidermis as they kept most of their skin appendages. On the other hand, while the sebaceous glands on the 28th day were still a rare occurrence in the PL grafts, in the PDA grafts their numbers were instead significantly higher (7.33 ± 0.58; $p < 0.05$) than in all the other groups.

The RNA-sequencing data were consistent with the above findings: the genes associate with the growth of normal epidermis (like *Krt27*, *Krt76* [50], and *Tcf 23* [51,52]) and hair follicles formation (like *Krt75* [53]) were significantly higher in the PDA group than those in PL group

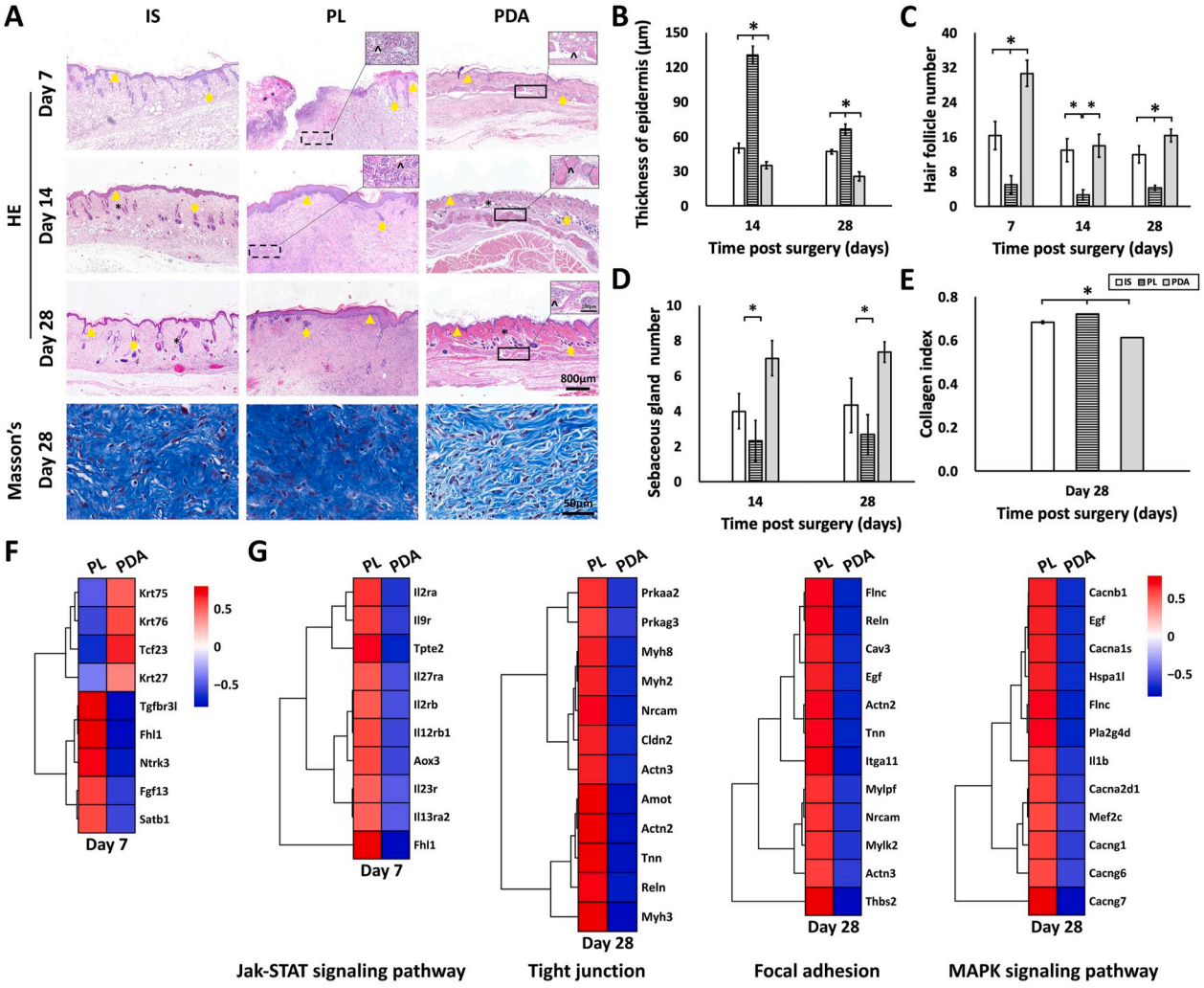

Fig. 5. (A) H&E staining of graft sections harvested at different time points showing epidermis (yellow triangles), hair follicles (yellow arrows), sebaceous glands (black stars), and implants (black ^ symbol). Masson's trichrome staining of skin grafts. (B) Epidermis thickness. (C) Quantification of hair follicles. (D) Quantification of sebaceous glands. (E) Quantification of collagen stain intensity in histological sections. (F) Heat Map of the genes associated with epidermal and skin appendage changes. (G) Heat Map of genes associated with fibrosis. From left to right: Jak-STAT's signalling pathway; tight junctions' pathway; focal adhesions' pathway; and MAPKs' signalling pathway, *$p < 0.05$.

(Fig. 5F) on the 7th day postoperatively. Whereas the expression of genes like *Fhl1* [54], *FGF13* [54], *TGFβR3l* [55] and *Satb1* [56], all of which were proven to connect with abnormal aspects of epidermal morphology, was most intense in the PL group.

Compare to unwounded skin, collagen fibers in scar tissue are densely packed, align linearly along direction of the tension, which results in myofibroblast hyperplasia and scar contraction. Masson's trichrome staining was applied to analyse collagen deposition and organization in the skin grafts (with the blue stained area representing the collagen). As shown in Fig. 5A, while the IS and PL groups were in a fibrotic state with dark blue dyed, compact arranged collagen fibers on the 28th day postoperatively, the PDA grafts were much like un-injured skin characterized by loosely packed collagen fibres arranged according to a "basket-weave" pattern. The results of the quantitative image analysis further supported these observations (Fig. 5E). The amount of collagen deposits was significantly higher in the PL (0.72 ± 0.01) grafts than in the IS (0.68 ± 0.01) grafts, whereas the quantity of collagen fibres (0.61 ± 0.01) was at its lowest level ($p < 0.05$) in the PDA grafts.

The KEGG enrichment analysis was used to understand the graft scarring mechanisms by revealing the signalling pathways involved in fibrosis (Fig. 5G). On the 7th day after the injury, the Jak-STAT signalling pathway was significantly enriched ($p = 0.0028$) [57–60] in the PL-*vs.*-PDA groups, and the differentially expressed genes were significantly upregulated (10/11) in the PL group. On the 28th day after the injury, a significant enrichment of the signalling pathways associated with tight junctions ($p = 0.0063$) [61], focal adhesions ($p = 0.0102$) [42,62], and MAPKs ($p = 0.0166$) [27] occurred in the PL-*vs.*-PDA groups. Conversely, the differentially expressed genes connected with tight junctions (12/12), focal adhesions (11/12), and MAPKs signalling pathways (12/13) were significantly down-regulated in the PDA group.

Among this, some profibrotic genes were found significantly down-regulated in the PDA grafts on the 7th and the 28th days (Fig. 5G), i.e. the *Il13rα2* gene, a known therapeutic target for TGF-β-driven pulmonary fibrosis [63]; the *Itgα11* gene, which encoded a collagen-binding integrin regulating intracellular collagen production [64] and, when overexpressed, inducing cardiac fibrosis and left ventricle hypertrophy [65]; the *Thbs2* gene, which specifically associated with the progression of liver fibrosis [42]; the *IL1β* gene, an effective pro-inflammatory cytokine promoting fibroblasts proliferation and collagen deposition [66,67]. These observations revealed as likely that PDA devices might mitigate wound fibrosis by inhibiting the expression and signalling pathways of the just mentioned genes. However, the role(s) of the profibrotic genes in our biomaterial-microenvironment settings warrant(s) further studies.

3.6. Skin graft neovascularization analyses

The after implantation survival of the grafts relies mainly on efficacious blood circulation, which supplies nutrients that are crucial to skin repair [68]. The development of a functional neovasculature at an early stage of implantation is associated with an enhanced maintenance of healthy skin grafts, which prevent scar formation and subsequent contraction in site.

Fig. 6A showed the grafts densities of the microvessels (as characterized by endothelialized lumens containing red blood cells) under a high-power field (HPF) microscope. At the earliest post-operative time point (the 3rd day), the microvessel number (Fig. 6B) in the PDA group (30.67 ± 3.06/HPF) was much higher than those in PL (17.33 ± 2.52/

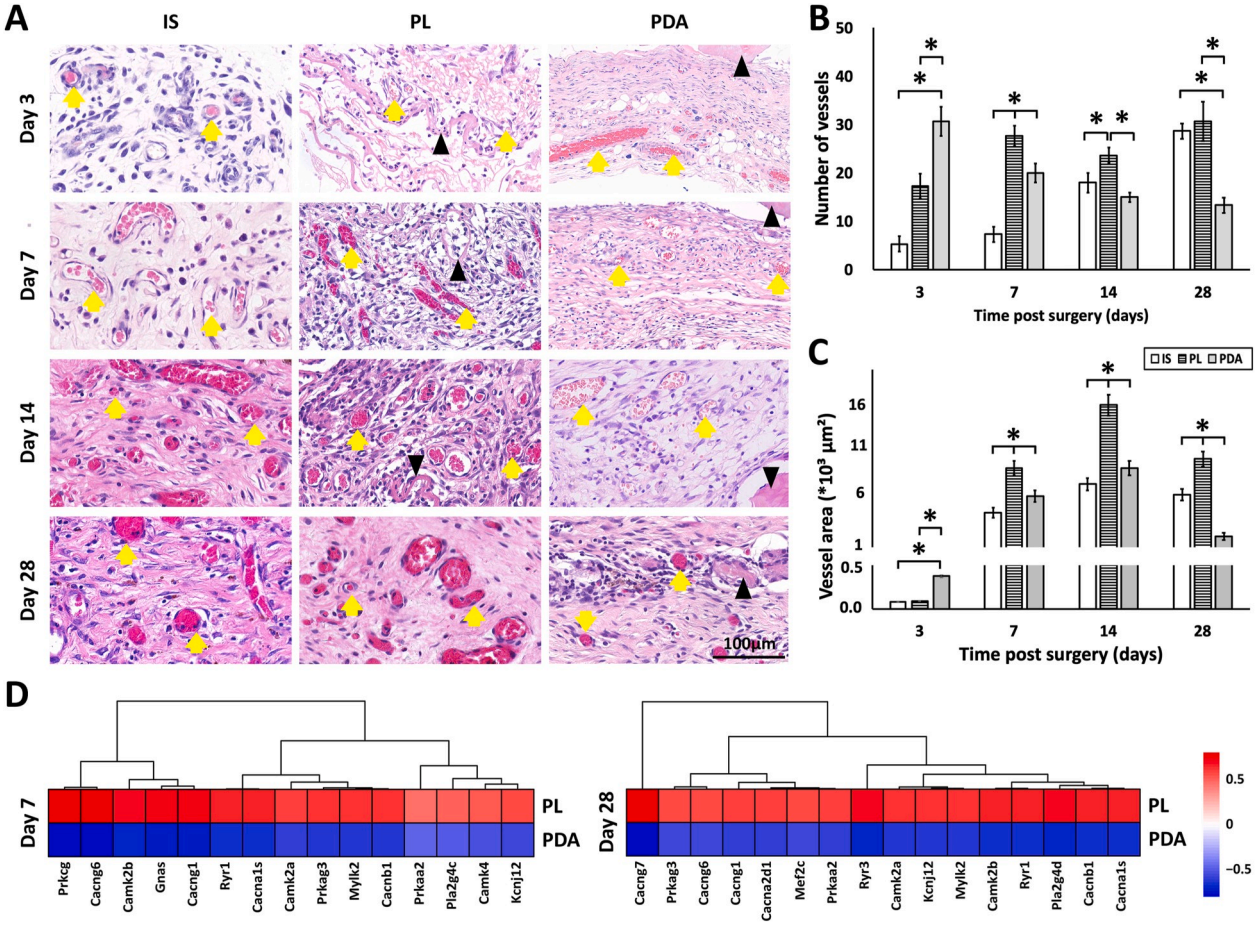

Fig. 6. (A) The H&E stained microvessels (yellow arrows) and implanted materials (black triangles) in the grafts on the 3rd, 7th, 14th, 28th days. (B) The quantification of microvessels' numbers. (C) The quantification of microvessels areas, *$p < 0.05$. (D) The heat map of the genes involved in oxytocin signalling pathway.

HPF) and in IS groups (5.33 ± 1.53/HPF) ($p < 0.05$). While the microvessel density values were significantly increased in the IS and PL groups up to the 7th day (7.33 ± 1.53/HPF and 27.67 ± 2.08/HPF) and to the 14th day (18.00 ± 2.00/HPF and 23.67 ± 1.53/HPF), a decreasing trend became manifest in the PDA group since the 7th day onwards (20.00 ± 2.00/HPF). By the 28th day, in the PDA group the vessel density was significantly lower (13.33 ± 1.53/HPF; $p < 0.05$) than those in the other grafts.

The degree of the grafts vascularization could be also defined by the microvessels' area as shown in Fig. 6C. On the 3rd day, in the PDA grafts the total vessels area (408.50 ± 32.33 μm^2/HPF) was significantly greater than those in the remaining groups. While the vessels area underwent a significant increase on the 7th and the 14th day, and a subsequent decrease on the 28th day in the remaining groups, the smallest vessel area was observed in the PDA grafts (2548.06 ± 30.96μm^2/HPF; $p < 0.05$).

As shown in Fig. 6D, the genes involved in oxytocin signalling pathway, which regulated the endothelial cell proliferation and directly stimulated the production of new vessels [33,69–73], were significantly upregulated in the PL group both on the 7th day 7 ($p = 1.489395e-08$, 15/17 significantly up-regulated genes) and the 28th day ($p = 7.637762e-08$, 12/13 significantly up-regulated genes). In particular, the *Grem1* [74] gene not only induced neoangiogenesis, but also advanced the progression of hepatic fibrosis [75]. The transcriptomics data were correlation with the increased vascularization level of the PL group on the post-operative 7th day and at later stages, indicating a phenomenon could be attributed to a persistent inflammation provoked by the necrotic cells [76].

3.7. Macrophage polarization in surgical sites

An inflammatory response will be evoked after skin wounding. Among all the immune cells involved in such a response, the subsequent changes of Mϕs phenotype (M1⇒M2) act as crucial determinants not only of wound repair regulation, but also of the material's incorporation and scarring [77,78]: the long existence of M1 macrophage would damage the tissue engineering materials and impair its ability to promote tissue regeneration, and M2 macrophage attributes to the adaptation of tissue engineering material and promotes tissue remodelling [79,80], but consistently increased M2 macrophages have been closely linked to hypertrophic scar at 14–28 days after wounding [81]. At all the selected time points, the Mϕs reaction of cluster of differentiation 68 (CD68), a pan-macrophage-positive marker, was intense in the PL grafts (Fig. 7A and B) and was typical of a predominating M1 (CCR7-positive) phenotype ($p < 0.05$). Conversely, on the 7th day after the surgery, PDA grafts exhibited a modest CD68 response and they predominantly belonged to a M1 profile (M2/M1 was 0.76 ± 0.07). Although the macrophages present in the wounds were of a mixed M1/M2 phenotype, an increasing proportion of M2 Mϕs was detected in PDA grafted wounds compared with those in IS and PL grafted ones since the 14th day onwards (on the 14th day, 2.01 ± 0.11; on the 28th day, 3.28 ± 0.22%; $p < 0.05$ in either instance). The reduced total number of macrophages and switch between phenotypes suggested that the PDA wounds be ready to move from a reparative stage characterized by re-epithelization and granulation tissue development towards a stable stage [27]. Whereas the unbalanced polarization toward M1 phenotype in PL grafts, caused by undesired biomaterial-wound interaction(s), might elicit a wound healing blighted by undesirable features [82–84].

The transcriptomics data further revealed the probable upstream

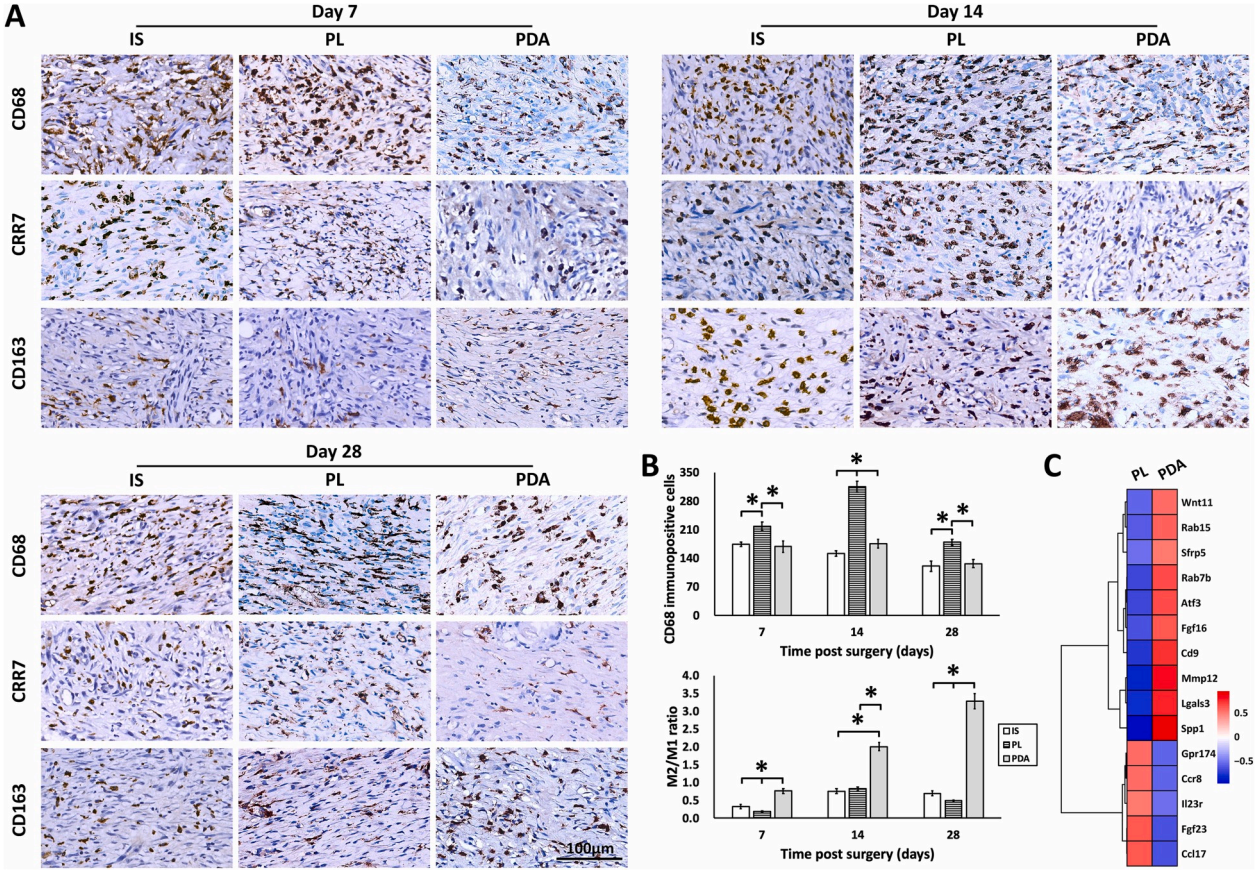

Fig. 7. (A) Macrophage polarization assessment of the compared groups on the 7th, 14th and 28th days post-operatively. The Mϕs phenotype within each section was assessed through immunohistochemical staining for CD68 (pan-Mϕs), CRR7 (M1 Mϕs), and CD163 (M2 Mϕs). (B) The quantification of Mϕs and ratios of M1: M2 percentages, *$p < 0.05$. (C) The heat map of the genes associated with inflammation and Mϕs polarization.

causes of this phenotype shift (Fig. 7C). On the post-operational 7th day, genes related to M1 polarization [85] like *Il23r* [86], *CCR8* [87], and *Gpr174* [76], which were known to correlate with disproportionate inflammatory responses [88] and various inflammatory diseases [86,89], were significantly upregulated in PL group. Meanwhile, the genes known to inhibit inflammatory reactions in obese subjects, such as *Sfrp5* [90], *Wnt11* [91], *Fgf 16* [92], *Rab7b* [93], *Rab 15*, *ATF3* [94], and *Cd9* [95], were significantly upregulated in the PDA group on the post-operational 7th day. These genes could not only modulate *NF-κB* in LPS-stimulated Mϕs [91], but also decrease monocyte infiltration, increase M1⇒M2 Mϕs phenotypic differentiation, and release anti-inflammatory cytokines associated with wound remodelling [92,93,95,96]. No Genetic differences were found on the 28th day. The reason could be that the genetic changes related to macrophage polarization occurred mainly at the early stages of wound healing. Therefore, the grafting "early stage" played a vital role in the whole graft take process [25].

4. Conclusion

Here we report a novel, anti-scarring method to assemble grafts of PDA using porcine dECMp, which recapitulate the latter's compositional and topological features. We proved that transplanting autologous IS along with an optimally crosslinked PDA device significantly reduced wound contraction and scarring in an immune competent, full-thickness wound model. The PDA-implanted group shows an efficient early revascularization, an increased polarization of macrophages to the M2 phenotype, better preserved skin functions, and a repair advancing effect whose upshot bore a closer morphological resemblance to normal skin. We also disclosed the basic transcriptional profiles of the STSG-engineered dermal biomaterial-wound complex in both the early and late stages of the healing process. PDA's preserved dermis-specific ECM cues and optimized mechanical properties, such as flexibility and elastic modulus, which collaboratively modulated endogenous signalling pathways, are likely to exert aforementioned therapeutically beneficial effects. which collaboratively modulated endogenous signalling pathways, are likely to exert aforementioned therapeutically beneficial effects. Together, our present results may help increase the understanding of how at the molecular level the IS and skin wounds respond to biomaterial stimuli and serve as a starting foundation for future improvements of biomaterials' anti-scarring properties and of their clinical translatability.

Declaration of competing interest

The authors declare that they have no known competing financial interests or personal relationships that could have appeared to influence the work reported in this paper.

Data availability

The authors declare that all data supporting the findings of this study are available within this article, its Supporting Information, and online deposited data (The mass spectrometry proteomics data: PXD020956, RNA-seq data: PRJNA642257).

CRediT authorship contribution statement

Lei Chen: Funding acquisition, Conceptualization, Formal analysis, Investigation, Methodology, Writing – original draft, Writing – review & editing. Zhiyong Li: Investigation, Methodology, Writing – original draft. Yongtai Zheng: Conceptualization, Methodology. Fei Zhou: Investigation. Jingling Zhao: Investigation and Qiyi Zhai: Investigation. Zhaoqiang Zhang: Writing – original draft. Tianrun Liu: Formal analysis, Transcriptome analysis, Writing – original draft. Yongming Chen: Funding acquisition, Project administration, Writing – review & editing. Shaohai Qi: Funding acquisition, Project administration, Conceptualization, Writing – review & editing.

Acknowledgements

We would like to acknowledge Dr. Yang Fu, Dr. Xujia Wu, Dr. Yanan Wang, Dr. Jianfeng Cao, Dr. Zhigang Chen, Dr. Jinyu Tan, Dr. Chi Zhang, Dr. Guanrui Liao, Dr. Yingtong Hou, Dr. Sifang Li (Department of Clinical Medicine, Zhongshan School of Medicine, Sun Yat-sen University) and Yanan Chen B.S. (Department of Burns, The First Affiliated Hospital, SunYat-Sen University) for their technical assistance in dECMp ink formulating and PDAs fabrication. The authors also want to thank Prof. Dr. Ubaldo Armato, M.D. in the Histology & Embryology Unit, University of Verona Medical School, and Dr. Wei Liu in the Institute of Mechanics, Chinese Academy of Sciences, for their careful reading of the manuscript and for several useful comment. This study was supported by the National Natural Science Foundation of China (NSFC: 81971856), the Guangdong Basic and Applied Basic Research Foundation (2020B1515020049), the Science and Technology Program of Guangzhou (201704020165), Ke lin New-star Plan (Y50177) of the First Affiliated Hospital of Sun Yat-sen University, and the Guangdong Innovative and Entrepreneurial Research Team Program (2013S086).

Appendix A. Supplementary data

Supplementary data to this article can be found online at https://doi.org/10.1016/j.bioactmat.2021.09.008.

References

[1] B. Sund, A.K. Arrow, New Developments in Wound Care, PJB Publications, London, 2000.
[2] J.C. Schneider, R. Holavanahalli, P. Helm, R. Goldstein, K. Kowalske, Contractures in burn injury: defining the problem, J. Burn Care Res. 27 (2006) 508–514, https://doi.org/10.1097/01.BCR.0000225994.75744.9D.
[3] K.M. Bombaro, L.H. Engrav, G.J. Carrougher, S.A. Wiechman, L. Faucher, B. A. Costa, D.M. Heimbach, F.P. Rivara, S. Honari, What is the prevalence of hypertrophic scarring following burns? Burns 29 (2003) 299–302, https://doi.org/10.1016/S0305-4179(03)00067-6.
[4] M. Chen, M. Przyborowski, F. Berthiaume, Stem cells for skin tissue engineering and wound healing, Crit. Rev. Biomed. Eng. 37 (2009) 399–421, https://doi.org/10.1615/critrevbiomedeng.v37.i4-5.50.
[5] K.C. Rustad, V.W. Wong, M. Sorkin, J.P. Glotzbach, M.R. Major, J. Rajadas, M. T. Longaker, G.C. Gurtner, Enhancement of mesenchymal stem cell angiogenic capacity and stemness by a biomimetic hydrogel scaffold, Biomaterials 33 (2012) 80–90, https://doi.org/10.1016/j.biomaterials.2011.09.041.
[6] C. Mazio, C. Casale, G. Imparato, F. Urciuolo, C. Attanasio, M. De Gregorio, F. Rescigno, P.A. Netti, Pre-vascularized dermis model for fast and functional anastomosis with host vasculature, Biomaterials 192 (2019) 159–170, https://doi.org/10.1016/j.biomaterials.2018.11.018.
[7] S. Zhong, Y. Zhang, C. Lim, Tissue scaffolds for skin wound healing and dermal reconstruction, Wiley Interdisciplinary Reviews: Nanomedicine and Nanobiotechnology 2 (2010) 510–525, https://doi.org/10.1002/wnan.100.
[8] W.-C. Yan, P. Davoodi, S. Vijayavenkataraman, Y. Tian, W.C. Ng, J.Y.H. Fuh, K. S. Robinson, C.-H. Wang, 3D bioprinting of skin tissue: from pre-processing to final product evaluation, Adv. Drug Deliv. Rev. 132 (2018) 270–295, https://doi.org/10.1016/j.addr.2018.07.016.
[9] J.R. Yu, J. Navarro, J.C. Coburn, B. Mahadik, J. Molnar, J.H. Holmes IV, A.J. Nam, J.P. Fisher, Current and future perspectives on skin tissue engineering: key features of biomedical research, translational assessment, and clinical application, Advanced Healthcare Materials 8 (2019) 1801471, https://doi.org/10.1002/adhm.201801471.
[10] T. Liu, C. Qiu, C. Ben, H. Li, S. Zhu, One-step approach for full-thickness skin defect reconstruction in rats using minced split-thickness skin grafts with Pelnac overlay, Burns Trauma 7 (2019) 19, https://doi.org/10.1186/s41038-019-0157-0.
[11] B. De Angelis, P. Gentile, E. Tati, D.J. Bottini, I. Bocchini, F. Orlandi, G. Pepe, C. D. Segni, G. Cervelli, V. Cervelli, One-stage reconstruction of scalp after full-thickness oncologic defects using a dermal regeneration template (Integra), BioMed Res. Int. 2015 (2015) 698385, https://doi.org/10.1155/2015/698385.
[12] J.Q. Coentro, E. Pugliese, G. Hanley, M. Raghunath, D.I. Zeugolis, Current and upcoming therapies to modulate skin scarring and fibrosis, Adv. Drug Deliv. Rev. 146 (2019) 37–59, https://doi.org/10.1016/j.addr.2018.08.009.
[13] D. Druecke, E.N. Lamme, S. Hermann, J. Pieper, P.S. May, H.U. Steinau, L. Steinstraesser, Modulation of scar tissue formation using different dermal regeneration templates in the treatment of experimental full-thickness wounds, Wound Repair Regen. 12 (2004) 518–527, https://doi.org/10.1111/j.1067-1927.2004.012504.x.

[14] L. Chen, Q. Xing, Q. Zhai, M. Tahtinen, F. Zhou, L. Chen, Y. Xu, S. Qi, F. Zhao, Pre-vascularization enhances therapeutic effects of human mesenchymal stem cell sheets in full thickness skin wound repair, Theranostics 7 (2017) 117–131, https://doi.org/10.7150/thno.17031.
[15] U. Wollina, U. Berger, G. Mahrle, Immunohistochemistry of porcine skin, Acta Histochem. Cytoc. 90 (1991) 87–91, https://doi.org/10.1016/S0065-1281(11)80166-2.
[16] T.L. Sellaro, A. Ranade, D.M. Faulk, G.P. McCabe, K. Dorko, S.F. Badylak, S. C. Strom, Maintenance of human hepatocyte function in vitro by liver-derived extracellular matrix gels, Tissue Eng. 16 (2010) 1075–1082, https://doi.org/10.1089/ten.TEA.2008.0587.
[17] B.S. Kim, Y.W. Kwon, J.-S. Kong, G.T. Park, G. Gao, W. Han, M.-B. Kim, H. Lee, J. H. Kim, D.-W. Cho, 3D cell printing of in vitro stabilized skin model and in vivo pre-vascularized skin patch using tissue-specific extracellular matrix bioink: a step towards advanced skin tissue engineering, Biomaterials 168 (2018) 38–53, https://doi.org/10.1016/j.biomaterials.2018.03.040.
[18] M. Kawecki, W. Łabuś, A. Klama-Baryla, D. Kitala, M. Kraut, J. Glik, M. Misiuga, M. Nowak, T. Bielecki, A. Kasperczyk, A review of decellurization methods caused by an urgent need for quality control of cell-free extracellular matrix' scaffolds and their role in regenerative medicine, J. Biomed. Mater. Res. B Appl. Biomater. 106 (2018) 909–923, https://doi.org/10.1002/jbm.b.33865.
[19] N.S. Gandhi, R.L. Mancera, The structure of glycosaminoglycans and their interactions with proteins, Chem. Biol. Drug Des. 72 (2008) 455–482, https://doi.org/10.1111/j.1747-0285.2008.00741.x.
[20] V. Hintze, A. Miron, S. Moeller, M. Schnabelrauch, H.-P. Wiesmann, H. Worch, D. Scharnweber, Sulfated hyaluronan and chondroitin sulfate derivatives interact differently with human transforming growth factor-β1 (TGF-β1), Acta Biomater. 8 (2012) 2144–2152, https://doi.org/10.1016/j.actbio.2012.03.021.
[21] S.F. Badylak, Xenogeneic extracellular matrix as a scaffold for tissue reconstruction, Transpl. Immunol. 12 (2004) 367–377, https://doi.org/10.1016/j.trim.2003.12.016.
[22] S. Yunoki, T. Suzuki, M. Takai, Stabilization of low denaturation temperature collagen from fish by physical cross-linking methods, J. Biosci. Bioeng. 96 (2003) 575–577, https://doi.org/10.1016/S1389-1723(04)70152-8.
[23] C.A. Miles, N.C. Avery, V.V. Rodin, A.J. Bailey, The increase in denaturation temperature following cross-linking of collagen is caused by dehydration of the fibres, JMBio 346 (2005) 551–556, https://doi.org/10.1016/j.jmb.2004.12.001.
[24] Y. Wang, R. Xu, W. He, Z. Yao, H. Li, J. Zhou, J. Tan, S. Yang, R. Zhan, G. Luo, Three-dimensional histological structures of the human dermis, Tissue Eng. C Methods 21 (2015) 932–944, https://doi.org/10.1089/ten.TEC.2014.0578.
[25] B.K. Sun, Z. Siprashvili, P.A. Khavari, Advances in skin grafting and treatment of cutaneous wounds, Science 346 (2014) 941–945, https://doi.org/10.1126/science.1253836.
[26] Q. Zhai, F. Zhou, M.M. Ibrahim, J. Zhao, X. Liu, J. Wu, L. Chen, S. Qi, An immune-competent rat split thickness skin graft model: useful tools to develop new therapies to improve skin graft survival, Am. J. Transl. Res. 10 (2018) 1600.
[27] S.T. Boyce, M.C. Glafkides, T.J. Foreman, J.F. Hansbrough, Reduced wound contraction after grafting of full-thickness burns with a collagen and chondroitin-6-sulfate (GAG) dermal skin substitute and coverage with biobrane, J. Burn Care Rehabil. 9 (1988) 364–370, https://doi.org/10.1097/00004630-198807000-00010.
[28] D.E. Discher, P. Janmey, Y.L. Wang, Tissue cells feel and respond to the stiffness of their substrate, Science 310 (2005) 1139–1143, https://doi.org/10.1126/science.1116995.
[29] A.K. Smiley, J.M. Klingenberg, B.J. Aronow, S.T. Boyce, W. Kitzmiller, D.M. Supp, Microarray analysis of gene expression in cultured skin substitutes compared with native human skin, J. Invest. Dermatol. 125 (2005) 1286–1301, https://doi.org/10.1111/j.0022-202X.2005.23971.x.
[30] N.S. Greaves, J. Morris, B. Benatar, T.A. Alonsorasgado, M. Baguneid, A. Bayat, Acute cutaneous wounds treated with human decellularised dermis show enhanced angiogenesis during healing, PloS One 10 (2015), e0113209, https://doi.org/10.1371/journal.pone.0113209.
[31] A. Aijaz, R. Faulknor, F. Berthiaume, R.M. Olabisi, Hydrogel microencapsulated insulin-secreting cells increase keratinocyte migration, epidermal thickness, collagen fiber density, and wound closure in a diabetic mouse model of wound healing, Tissue Eng. 21 (2015) 2723–2732, https://doi.org/10.1089/ten.tea.2015.0069.
[32] N. Noiseux, M. Borie, A. Desnoyers, A. Menaouar, L.M. Stevens, S. Mansour, B. A. Danalache, D.C. Roy, M. Jankowski, J. Gutkowska, Preconditioning of stem cells by oxytocin to improve their therapeutic potential, Endocrinology 153 (2012) 5361–5372, https://doi.org/10.1210/en.2012-1402.
[33] M. Cattaneo, B. Chini, L. Vicentini, Oxytocin stimulates migration and invasion in human endothelial cells, Br. J. Pharmacol. 153 (2008) 728–736, https://doi.org/10.1038/sj.bjp.0707609.
[34] E.C. Keeley, B. Mehrad, R.M. Strieter, Chemokines as mediators of tumor angiogenesis and neovascularization, Exp. Cell Res. 317 (2011) 685–690, https://doi.org/10.1016/j.yexcr.2010.10.020.
[35] E.C. Keeley, B. Mehrad, R.M. Strieter, Chemokines as mediators of neovascularization, Arterioscler. Thromb. Vasc. Biol. 28 (2008) 1928–1936, https://doi.org/10.1161/atvbaha.108.162925.
[36] J.J. O'Shea, D.M. Schwartz, A.V. Villarino, M. Gadina, I.B. McInnes, A. Laurence, The JAK-STAT pathway: impact on human disease and therapeutic intervention, Annu. Rev. Med. 66 (2015) 311–328, https://doi.org/10.1146/annurev-med-051113-024537.
[37] M.D. Scuron, B.L. Fay, A.J. Connell, M.T. Peel, P.A. Smith, Ruxolitinib cream has dual efficacy on pruritus and inflammation in experimental dermatitis, Front. Immunol. 11 (2020) 620098, https://doi.org/10.3389/fimmu.2020.620098.
[38] C.G. Lin, S.J. Leu, N. Chen, C.M. Tebeau, S.X. Lin, C.Y. Yeung, L.F. Lau, CCN3 (NOV) is a novel angiogenic regulator of the CCN protein family, J. Biol. Chem. 278 (2003) 24200–24208, https://doi.org/10.1074/jbc.M302028200.
[39] X.Y. Zeng, Y.Q. Zhang, X.M. He, L.Y. Wan, H. Wang, Y.R. Ni, J. Wang, J.F. Wu, C. B. Liu, Suppression of hepatic stellate cell activation through downregulation of gremlin1 expression by the miR-23b/27b cluster, Oncotarget 7 (2016) 86198–86210, https://doi.org/10.18632/oncotarget.13365.
[40] J. Shi, M. Barakat, D. Chen, L. Chen, Bicellular tight junctions and wound healing, Int. J. Mol. Sci. 19 (2018), https://doi.org/10.3390/ijms19123862.
[41] A. Leask, Focal adhesion kinase: a key mediator of transforming growth factor beta signaling in fibroblasts, Adv. Wound Care 2 (2013) 247–249, https://doi.org/10.1089/wound.2012.0363.
[42] W. Chen, X. Wu, X. Yan, A. Xu, A. Yang, H. You, Multitranscriptome analyses reveal prioritized genes specifically associated with liver fibrosis progression independent of etiology, Am. J. Physiol. Gastrointest. Liver Physiol. 316 (2019) G744–G754, https://doi.org/10.1152/ajpgi.00339.2018.
[43] Q.C. Du, D.Z. Zhang, X.J. Chen, G. Lan-Sun, M. Wu, W.L. Xiao, The effect of p38MAPK on cyclic stretch in human facial hypertrophic scar fibroblast differentiation, PloS One 8 (2013), e75635, https://doi.org/10.1371/journal.pone.0075635.
[44] Y. Li, W. Zhang, J. Gao, J. Liu, H. Wang, J. Li, X. Yang, T. He, H. Guan, Z. Zheng, S. Han, M. Dong, J. Han, J. Shi, D. Hu, Adipose tissue-derived stem cells suppress hypertrophic scar fibrosis via the p38/MAPK signaling pathway, Tem Cell Research & Therapy 7 (2016) 102, https://doi.org/10.1186/s13287-016-0356-6.
[45] S. Fichtner-Feigl, W. Strober, K. Kawakami, R.K. Puri, A. Kitani, IL-13 signaling through the IL-13alpha2 receptor is involved in induction of TGF-beta1 production and fibrosis, Nat. Med. 12 (2006) 99–106, https://doi.org/10.1038/nm1332.
[46] S.N. Popova, M. Barczyk, C.F. Tiger, W. Beertsen, P. Zigrino, A. Aszodi, N. Miosge, E. Forsberg, D. Gullberg, Alpha11 beta1 integrin-dependent regulation of periodontal ligament function in the erupting mouse incisor, Mol. Cell Biol. 27 (2007) 4306–4316, https://doi.org/10.1128/mcb.00041-07.
[47] U. Lappalainen, J.A. Whitsett, S.E. Wert, J.W. Tichelaar, K. Bry, Interleukin-1 beta causes pulmonary inflammation, emphysema, and airway remodeling in the adult murine lung, Am. J. Respir. Cell Mol. Biol. 32 (2005) 311–318, https://doi.org/10.1165/rcmb.2004-0309OC.
[48] S.B. Amjad, R. Carachi, M. Edward, Keratinocyte regulation of TGF-β and connective tissue growth factor expression: a role in suppression of scar tissue formation, Wound Repair Regen. 15 (2007) 748–755, https://doi.org/10.1111/j.1524-475X.2007.00281.x.
[49] B. Li, C. Gao, J.S. Diao, D.L. Wang, F.F. Chu, Y. Li, G. Wang, S.Z. Guo, W. Xia, Aberrant Notch signalling contributes to hypertrophic scar formation by modulating the phenotype of keratinocytes, Exp. Dermatol. 25 (2016) 137–142, https://doi.org/10.1111/exd.12897.
[50] T. Ditommaso, D.L. Cottle, H.B. Pearson, H. Schluter, P. Kaur, P.O. Humbert, I. M. Smyth, Keratin 76 is required for tight junction function and maintenance of the skin barrier, PLoS Genet. 10 (2014), e1004706, https://doi.org/10.1371/journal.pgen.1004706.
[51] C.F. Guerrerojuarez, A.A. Astrowski, R. Murad, C.T. Dang, V.O. Shatrova, A. Astrowskaja, C.H. Lim, R. Ramos, X. Wang, Y. Liu, Wound regeneration deficit in rats correlates with low morphogenetic potential and distinct transcriptome profile of epidermis, J. Invest. Dermatol. 138 (2018) 1409–1419, https://doi.org/10.1016/j.jid.2017.12.030.
[52] P.L. Vu, R. Takatori, T. Iwamoto, Y. Akagi, H. Satsu, M. Totsuka, K. Chida, K. Sato, M. Shimizu, Effects of food-derived collagen peptides on the expression of keratin and keratin-associated protein genes in the mouse skin, skin pharmacol, Physiol. 28 (2015) 227–235, https://doi.org/10.1159/000369830.
[53] J. Chen, K. Jaeger, Z. Den, P.J. Koch, J.P. Sundberg, D.R. Roop, Mice expressing a mutant Krt75 (K6hf) allele develop hair and nail defects resembling pachyonychia congenita, J. Invest. Dermatol. 128 (2008) 270–279, https://doi.org/10.1038/sj.jid.5701038.
[54] M. Kawano, S. Suzuki, M. Suzuki, J. Oki, T. Imamura, Bulge- and basal layer-specific expression of fibroblast growth factor-13 (FHF-2) in mouse skin, J. Invest. Dermatol. 122 (2004) 1084–1090, https://doi.org/10.1111/j.0022-202X.2004.22514.x.
[55] S.M. Corley, V. Mendozareinoso, N. Giles, E.S. Singer, J.E.A. Common, M. R. Wilkins, A. Beverdam, Plau and Tgfbr3 are YAP-regulated genes that promote keratinocyte proliferation, Cell Death Dis. 9 (2018) 1106, https://doi.org/10.1038/s41419-018-1141-5.
[56] M.Y. Fessing, A.N. Mardaryev, M.R. Gdula, A.A. Sharov, T.Y. Sharova, V. Rapisarda, K.B. Gordon, A.D. Smorodchenko, K. Poterlowicz, G. Ferone, P63 regulates satb1 to control tissue-specific chromatin remodeling during development of the epidermis, J. Cell Biol. 194 (2011) 825–839, https://doi.org/10.1083/jcb.201101148.
[57] G. Soldevila, E.A. Garciazepeda, The role of the Jak-Stat pathway in chemokine-mediated signaling in T lymphocytes, Signal Transduct. 7 (2007) 427–438, https://doi.org/10.1002/sita.200700144.
[58] D.A. Harrison, The JAK/STAT pathway, Cold Spring Harb. Perspect. Biol. 4 (2012) a011205, https://doi.org/10.1101/cshperspect.a011205.
[59] A.M. Lakner, C.C. Moore, A.A. Gulledge, L.W. Schrum, Daily genetic profiling indicates JAK/STAT signaling promotes early hepatic stellate cell transdifferentiation, World J. Gastroenterol. 16 (2010) 5047–5056, https://doi.org/10.3748/wjg.v16.i40.5047.

[60] Y. Belacortu, N. Paricio, Drosophila as a model of wound healing and tissue regeneration in vertebrates, Dev. Dynam. 240 (2011) 2379–2404, https://doi.org/10.1002/dvdy.22753.
[61] J. Shi, M. Barakat, D. Chen, L. Chen, Bicellular tight junctions and wound healing, Int. J. Mol. Sci. 19 (2018) 3862, https://doi.org/10.3390/ijms19123862.
[62] A. Leask, Focal adhesion kinase: a key mediator of transforming growth factor beta signaling in fibroblasts, Adv. Wound Care 2 (2013) 247–249, https://doi.org/10.1089/wound.2012.0363.
[63] S. Fichtnerfeigl, W. Strober, K. Kawakami, R.K. Puri, A. Kitani, IL-13 signaling through the IL-13alpha2 receptor is involved in induction of TGF-beta1 production and fibrosis, Nat. Med. 12 (2006) 99–106, https://doi.org/10.1038/nm1332.
[64] S.N. Popova, M. Barczyk, C. Tiger, W. Beertsen, P. Zigrino, A. Aszodi, N. Miosge, E. Forsberg, D. Gullberg, Alpha11 beta1 integrin-dependent regulation of periodontal ligament function in the erupting mouse incisor, Mol. Cell Biol. 27 (2007) 4306–4316.
[65] A. Romaine, I.W. Sorensen, C. Zeltz, N. Lu, P.M. Erusappan, A.O. Melleby, L. Zhang, B. Bendiksen, E.L. Robinson, J.M. Aronsen, Overexpression of integrin α11 induces cardiac fibrosis in mice, Acta Physiol. 222 (2018), e12932, https://doi.org/10.1111/apha.12932.
[66] U. Lappalainen, J.A. Whitsett, S.E. Wert, J.W. Tichelaar, K. Bry, Interleukin-1β causes pulmonary inflammation, emphysema, and airway remodeling in the adult murine lung, Am. J. Respir. Cell Mol. Biol. 32 (2005) 311–318.
[67] K. Tominaga, T. Yoshimoto, K. Torigoe, M. Kurimoto, K. Matsui, T. Hada, H. Okamura, K. Nakanishi, IL-12 synergizes with IL-18 or IL-1β for IFN-γ production from human T cells, Int. Immunol. 12 (2000) 151–160, https://doi.org/10.1093/intimm/12.2.151.
[68] E.A. Azzopardi, D.E. Boyce, W.A. Dickson, E. Azzopardi, J.H.E. Laing, I. S. Whitaker, K. Shokrollahi, Application of topical negative pressure (vacuum-assisted closure) to split-thickness skin grafts: a structured evidence-based review, Ann. Plast. Surg. 70 (2013) 23–29, https://doi.org/10.1097/SAP.0b013e31826eab9e.
[69] N. Noiseux, M. Borie, A. Desnoyers, A. Menaouar, L.M. Stevens, S. Mansour, B. A. Danalache, D. Roy, M. Jankowski, J. Gutkowska, Preconditioning of stem cells by oxytocin to improve their therapeutic potential, Endocrinology 153 (2012) 5361–5372, https://doi.org/10.1210/en.2012-1402.
[70] E.C. Keeley, B. Mehrad, R.M. Strieter, Chemokines as mediators of tumor angiogenesis and neovascularization, Exp. Cell Res. 317 (2011) 685–690, https://doi.org/10.1016/j.yexcr.2010.10.020.
[71] E.C. Keeley, B. Mehrad, R.M. Strieter, Chemokines as mediators of neovascularization, Atertio. Thromb. Vasc. Biol. 28 (2008) 1928–1936, https://doi.org/10.1161/ATVBAHA.108.162925.
[72] C.G. Lin, S. Leu, N. Chen, C.M. Tebeau, S. Lin, C. Yeung, L.F. Lau, CCN3 (NOV) is a novel angiogenic regulator of the CCN protein family, J. Biol. Chem. 278 (2003) 24200–24208, https://doi.org/10.1074/jbc.M302028200.
[73] A. Barzelay, J. Benshoshan, M. Entinmeer, S. Mayselauslender, A. Afek, I. Barshack, G. Keren, J. George, A potential role for islet-1 in post-natal angiogenesis and vasculogenesis, Thromb. Haemostasis 103 (2009) 188–197, https://doi.org/10.1160/TH09-07-0433.
[74] S. Mitola, C. Ravelli, E. Moroni, V. Salvi, D. Leali, K. Ballmerhofer, L. Zammataro, M. Presta, Gremlin is a novel agonist of the major proangiogenic receptor VEGFR2, Blood 116 (2010) 3677–3680, https://doi.org/10.1182/blood-2010-06-291930.
[75] X. Zeng, Y. Zhang, X. He, L. Wan, H. Wang, Y. Ni, J. Wang, J. Wu, C. Liu, Suppression of hepatic stellate cell activation through downregulation of gremlin1 expression by the miR-23b/27b cluster, Oncotarget 7 (2016) 86198–86210.
[76] S. Aarabi, M.T. Longaker, G.C. Gurtner, Hypertrophic scar formation following burns and trauma: new approaches to treatment, PLoS Med. 4 (2007) e234, https://doi.org/10.1371/journal.pmed.0040234.
[77] K.L. Spiller, T.J. Koh, Macrophage-based therapeutic strategies in regenerative medicine, Adv. Drug Deliv. Rev. 122 (2017) 74–83, https://doi.org/10.1016/j.addr.2017.05.010.
[78] P.L. Graney, E.B. Lurier, K.L. Spiller, Biomaterials and bioactive factor delivery systems for the control of macrophage activation in regenerative medicine, ACS Biomater. Sci. Eng. 4 (2017) 1137–1148, https://doi.org/10.1021/acsbiomaterials.6b00747.
[79] B.M. Sicari, J.L. Dziki, B.F. Siu, C.J. Medberry, C.L. Dearth, S.F. Badylak, The promotion of a constructive macrophage phenotype by solubilized extracellular matrix, Biomaterials 35 (2014) 8605–8612, https://doi.org/10.1016/j.biomaterials.2014.06.060.
[80] H. Kang, S.H.D. Wong, Q. Pan, G. Li, L. Bian, Anisotropic ligand nanogeometry modulates the adhesion and polarization state of macrophages, Nano Lett. 19 (2019) 1963–1975, https://doi.org/10.1021/acs.nanolett.8b05150.
[81] Y. Zhu, X. Li, J. Chen, T. Chen, Z. Shi, M. Lei, Y. Zhang, P. Bai, Y. Li, X. Fei, The pentacyclic triterpene Lupeol switches M1 macrophages to M2 and ameliorates experimental inflammatory bowel disease, Int. Immunopharm. 30 (2016) 74–84, https://doi.org/10.1016/j.intimp.2015.11.031.
[82] P.J. Murray, T.A. Wynn, Protective and pathogenic functions of macrophage subsets, Nat. Rev. Immunol. 11 (2011) 723–737, https://doi.org/10.1038/nri3073.
[83] A. Mantovani, S.K. Biswas, M.R. Galdiero, A. Sica, M. Locati, Macrophage plasticity and polarization in tissue repair and remodelling, J. Pathol. 229 (2013) 176–185, https://doi.org/10.1002/path.4133.
[84] A.S. Macleod, J.N. Mansbridge, The innate immune system in acute and chronic wounds, Adv. Wound Care 5 (2016) 65–78, https://doi.org/10.1089/wound.2014.0608.
[85] T. Oshio, R. Kawashima, Y.I. Kawamura, T. Hagiwara, N. Mizutani, T. Okada, T. Otsubo, K. Inagakiohara, A. Matsukawa, T. Haga, Chemokine receptor CCR8 is required for lipopolysaccharide-triggered cytokine production in mouse peritoneal macrophages, PloS One 9 (2014), e94445, https://doi.org/10.1371/journal.pone.0094445.
[86] R.H. Duerr, K.D. Taylor, S.R. Brant, J.D. Rioux, M.S. Silverberg, M.J. Daly, A. H. Steinhart, C. Abraham, M. Regueiro, A.M. Griffiths, A genome-wide association study identifies IL23R as an inflammatory bowel disease gene, Science 314 (2006) 1461–1463, https://doi.org/10.1126/science.1135245.
[87] M.K. Reimer, C. Brange, A. Rosendahl, CCR8 signaling influences Toll-like receptor 4 responses in human macrophages in inflammatory diseases, Clin. Vaccine Immunol. 18 (2011) 2050–2059, https://doi.org/10.1128/CVI.05275-11.
[88] E.A. Fitzpatrick, X. Han, Z. Xiao, L.D. Quarles, Role of fibroblast growth factor-23 in innate immune responses, Front. Endocrinol. 9 (2018) 320, https://doi.org/10.3389/fendo.2018.00320.
[89] T. Komatsu-Fujii, Y. Chinuki, H. Niihara, K. Hayashida, M. Ohta, R. Okazaki, S. Kaneko, E. Morita, The thymus and activation-regulated chemokine (TARC) level in serum at an early stage of a drug eruption is a prognostic biomarker of severity of systemic inflammation, Allergol. Int. 67 (2018) 90–95, https://doi.org/10.1016/j.alit.2017.06.001.
[90] N. Ouchi, A. Higuchi, K. Ohashi, Y. Oshima, N. Gokce, R. Shibata, Y. Akasaki, A. Shimono, K. Walsh, Sfrp5 is an anti-inflammatory adipokine that modulates metabolic dysfunction in obesity, Science 329 (2010) 454–457, https://doi.org/10.1126/science.1188280.
[91] Y. Morishita, K. Kobayashi, E. Klyachko, K. Jujo, K. Maeda, D.W. Losordo, T. Murohara, Wnt11 gene therapy with adeno-associated virus 9 improves recovery from myocardial infarction by modulating the inflammatory response, Sci. Rep. 6 (2016) 21705, https://doi.org/10.1038/srep21705.
[92] Y. Hu, L. Li, L. Shen, H. Gao, F. Yu, W. Yin, W. Liu, FGF-16 protects against adverse cardiac remodeling in the infarct diabetic heart, Am. J. Transl. Res. 9 (2017) 1630–1640.
[93] Y. Wang, T. Chen, C. Han, D. He, H. Liu, H. An, Z. Cai, X. Cao, Lysosome-associated small Rab GTPase Rab7b negatively regulates TLR4 signaling in macrophages by promoting lysosomal degradation of TLR4, Blood 110 (2007) 962–971, https://doi.org/10.1182/blood-2007-01-066027.
[94] H. Luo, J. Wang, C. Qiao, X. Zhang, W. Zhang, N. Ma, ATF3 inhibits tenascin-C-induced foam cell formation in LPS-stimulated THP-1 macrophages by suppressing TLR-4, J. Atherosclerosis Thromb. 22 (2015) 1214–1223, https://doi.org/10.5551/jat.28415.
[95] M. Suzuki, I. Tachibana, Y. Takeda, P. He, S. Minami, T. Iwasaki, H. Kida, S. Goya, T. Kijima, M. Yoshida, Tetraspanin CD9 negatively regulates lipopolysaccharide-induced macrophage activation and lung inflammation, J. Immunol. 182 (2009) 6485–6493, https://doi.org/10.4049/jimmunol.0802797.
[96] H. Sha, D. Zhang, Y. Zhang, Y. Wen, Y. Wang, ATF3 promotes migration and M1/M2 polarization of macrophages by activating tenascin-C via Wnt/β-catenin pathway, Mol. Med. Rep. 16 (2017) 3641–3647, https://doi.org/10.3892/mmr.2017.6992.